Phys Chem Minerals (1985) 12:370–378

PHYSICS AND CHEMISTRY OF MINERALS

Magnetic Properties of Sheet Silicates; 2:1:1 Layer Minerals

O. Ballet*, J.M.D. Coey and K.J. Burke
Department of Pure and Applied Physics, Trinity College, Dublin 2, Ireland

Abstract. Magnetization, susceptibility and Mössbauer spectra are reported for representative chlorite samples with differing iron content. The anisotropy of the susceptibility and magnetization of a clinochlore crystal is explained using the trigonal effective crystal-field model developed earlier for 1:1 and 2:1 layer silicates, with a splitting of the T_{2g} triplet of 1,120 K. Predominant exchange interactions in the iron-rich samples are ferromagnetic with $J=1.2$ K, as for other trioctahedral ferrous minerals. A peak in the susceptibility of thuringite occurs at $T_m=5.5$ K, and magnetic hyperfine splitting appears at lower temperatures in the Mössbauer spectrum. However neutron diffraction reveals no long-range magnetic order in thuringite (or biotite, which behaves similarly). The only magnetic contribution to the diffraction pattern at 1.6 K is increased small angle scattering ($q<0.4$ Å^{-1}). A factor favouring this random ferromagnetic ground state over the planar antiferromagnetic state of greenalite and minnesotaite is the presence of pairs of ferric ions on adjacent sites, in conjunction with magnetic vacancies in the octahedral sheets. Monte Carlo simulations of the magnetic ground state of the sheets illustrate how long range ferromagnetic order may be destroyed by vortices forming around the Fe^{3+}—Fe^{3+} pairs.

Introduction

Magnetic order is known to occur in iron-rich sheet silicates at temperatures in the liquid helium range. Our previous studies have dealt with the 1:1 (Coey et al. 1981) and 2:1 (Ballet and Coey 1982) structural families where strong hard-axis anisotropy due to the Fe^{2+} ions in trigonally distorted octahedral sites has been described. These papers will be referred to as I and II, respectively. The sheet structures have much greater iron-iron distances between planes than within them, which gives their magnetic properties a markedly two-dimensional character.

In the present paper, we complete our survey of the magnetic properties of natural samples of sheet silicates with a study of 2:1:1 layer and related minerals (the chlorite group); we also draw some general conclusions. The structure, shown in Fig. 1, consists of 2:1 sandwich layers intercalated with single sheets of cations octahedrally coordinated by hydroxyls. The two layers are often referred to as the talc $[Si]_4\{Mg_3\}O_{10}(OH)_2$ and brucite $\{Mg_3\}(OH)_6$ layers, although they are not electrically neutral in chlorites. Substitution of trivalent ions for Mg in the brucite layers is compensated by replacement of Si by Al in the tetrahedral sheets of the talc layers (Bailey 1980).

The general formula for a trioctahedral chlorite is

$$[Si_{4-x}Al_x]\{R^{2+}_{6-x}R^{3+}_x\}O_{10}(OH)_8 \quad (1)$$

where R^{2+} is usually Mg or Fe^{2+}, and R^{3+} is usually Al or Fe^{3+}. Typically $x\simeq 1$. The different brackets [ ] and { } are used to denote tetrahedral and octahedral sites respectively. Chlorite minerals rich in ferrous iron are fairly common, and a nomenclature has been devised which is based on the value of x and the Fe^{2+}/R^{2+} ratio (Foster 1962). Many iron-rich chlorites are indistinguishable from minerals of the trioctahedral 1:1 (serpentine) family on the basis of their chemical composition. The characteristic of a true chlorite is a 14 Å 001 X-ray reflection, whereas the first reflection from the serpentines is at 7 Å. Structurally, however, the chlorites are closely related to the 2:1 layer minerals, with an extra cation site ($M3$) in the interlayer positions.

The iron content of a chlorite sample is reflected in the lattice parameters, the b parameter in particular. Iron

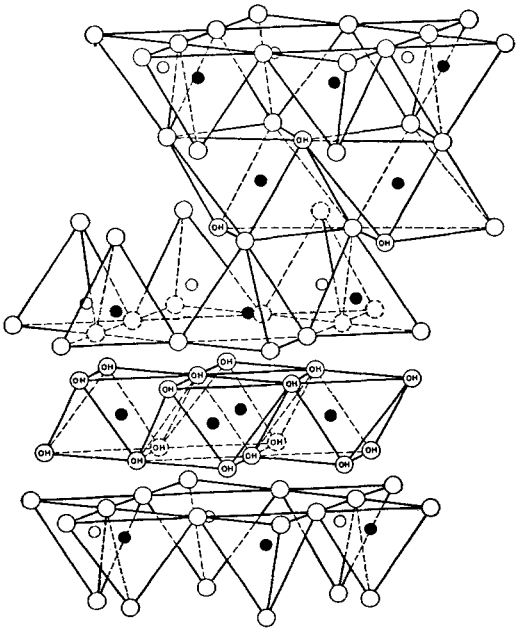

Fig. 1. Fragment of the 2:1:1 layer

* *Present Adress:* Institut für Kristallographie und Mineralogie, Universität Frankfurt am Main, 6000 Frankfurt, West Germany

enters the octahedral sites, and its distribution between talc and brucite layers may be determined, in principle, from the intensities of 00*l* X-ray reflections (Petruk 1964), although there are some practical difficulties in determining these with sufficient accuracy (Brown and Brindley 1980). We will show here how neutron scattering can be useful in this respect. Mössbauer spectroscopy is usually quite informative for determining the valence state and cation distribution of iron in silicates (Coey 1984), but in the case of chlorites it is found that there is no structure to the ferrous quadrupole doublet, and that its hyperfine parameters are practically unaffected by the chemical composition (Hayashi et al. 1972). In contrast to trioctahedral 2:1 minerals, it appears to be impossible to distinguish ferrous iron in *M*1 (*trans* hydroxyls) and *M*2 (*cis* hydroxyls) sites in the talc layer (Blaauw et al. 1980). It has been suggested, partly on the basis of Mössbauer spectra of oxidized samples, that only the ferric form of iron enters the brucite layer (Borggard et al. 1982), but other authors (Goodman and Bain 1979) suggested that ferrous iron occupies the brucite sites as well. More recent work on these materials favours both Fe^{2+} and Fe^{3+} substitution there (Townsend et al. unpublished). In fact the presence of Fe^{2+} in *M*3 sites is thought to be necessary to explain the chemical transformation of chlorite into vermiculite (Ross and Kodama 1976).

Little has been published on the magnetic properties of chlorites. The room temperature susceptibility of pure samples with differing iron content has been shown to vary roughly as expected from the Curie law (Petruk 1965). Mössbauer spectra at 4.2 and 1.5 K show hyperfine split patterns coexisting with paramagnetic quadrupole doublets (Ballet 1979, Kodama et al. 1982, Townsend et al. unpublished).

In the following sections we examine the paramagnetism as a function of temperature and the collective magnetic behaviour at low temperatures of some representative chlorites, including one single-crystal sample. Magnetic properties, Mössbauer spectra and magnetic neutron diffraction patterns are compared with those of minnesotaite (a ferrous talc) (Ballet et al. 1985, Townsend et al. 1985), biotite or synthetic ferrobrucite $\{Fe_xMg_{1-x}\}(OH)_2$. Some general conclusions are drawn concerning the influence of the iron cation distribution on the magnetic order in trioctahedral sheet silicates.

Materials

From data on ten chlorites, we selected five representative trioctahedral samples for further study. In order of decreasing iron content these were the following.

1. A *thuringite* from Ishpeming, Michigan composed of tiny green crystals was obtained through Wards Natural Science Establishment (Rochester, New York). The formula derived from emission spectroscopy and X-ray fluorescence was

$$[Si_{2.64}Al_{1.36}]\{Al_{1.08}Fe^{2+}_{2.75}Fe^{3+}_{0.92}Mg_{0.93}\}O_{10}(OH)_8.$$

X-ray diffraction shows it to be of the IIb polytype, like more than 80% of true chlorites (Bailey 1980), with lattice parameters $a=5.42$ Å, $b=9.35$ Å, $c=14.25$ Å, $\beta=97.3$ Å.

2. A *chamosite* from Niger in the form of a fine, clay-grade powder mixed with analcime was obtained from the Centre de Sédimentologie et Géochimie de la Surface, Strasbourg. Attributing all the sodium found by chemical analysis to the latter phase yields the formula

$$[Si_{2.97}Al_{1.03}]\{Al_{1.50}Fe^{2+}_{2.41}Fe^{3+}_{0.33}Mg_{0.83}Ti_{0.35}\}O_{10}(OH)_8.$$

X-ray diffraction showns no 14 Å reflection, the first peak being at 7.10 Å, so this material is not really a chlorite at all, but a 7 Å, 1:1 layer serpentine mineral. It is included in the present study to see to what extent, if at all, it can be distinguished from the true 2:1:1 layer chlorites on the basis of its magnetic properties.

3. A *ripidolite*, from Flagstaff Hill, California was obtained through the Source Clay Minerals Repository (sample CCA-1). The composition of this material has recently been reported (Borggaard et al. 1982) as

$$[Si_{2.68}Al_{1.33}]\{Al_{1.17}Fe^{2+}_{1.95}Fe^{3+}_{0.18}Mg_{2.69}\}O_{10}(OH)_8.$$

X-ray diffraction shows it to be the IIb polytype with $a=5.34$ Å, $b=9.26$ Å, $c=14.26$ Å, $\beta=97$ Å.

4. A *clinochlore* from Calaveras County, California, also obtained from Wards, included small crystals ($\simeq 2\times 2\times 0.2$ mm^3) which were used to determine the anisotropy of the susceptibility. Emission and X-ray fluorescence analysis give the formula

$$[Si_{3.00}Al_{1.00}]\{Al_{0.96}Fe^{2+}_{0.48}Fe^{3+}_{0.14}Mg_{4.30}\}O_{10}(OH)_8.$$

According to X-ray diffraction, it is also a IIb polytype with parameters $a=5.33$ Å, $b=9.24$ Å, $c=14.37$ Å and $\beta=97.2$ Å.

5. An *amesite* from the Saranovskoye chromite deposit in the Urals was obtained from the Smithsonian Institute, Washington (US National Museum, No 103312). It was mixed with spinel, and no chemical analysis was obtained. The low temperature magnetization curve and Mössbauer absorption areas showed that the iron content was small, i.e. $Fe^{2+}_{0.04}Fe^{3+}_{0.02}$ in octahedral sites. Amesite is an alumin-

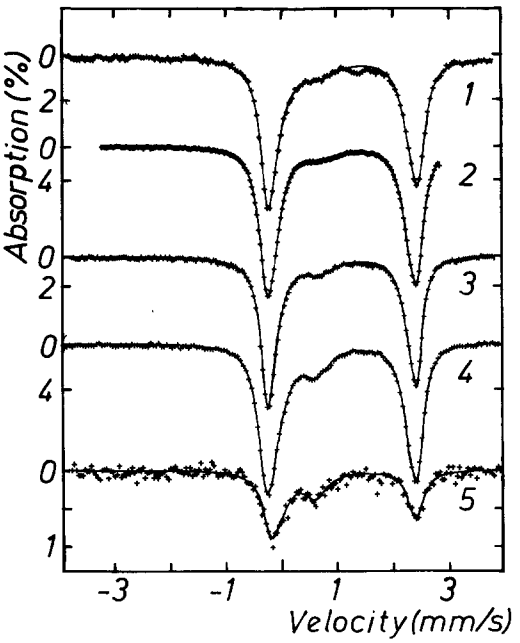

Fig. 2. Room temperature Mössbauer spectra of thuringite (1), chamosite (2), ripidolite (3), clinochlore (4) and amesite (5)

Table 1. Hyperfine parameters obtained from two-doublets fits to room-temperature Mössbauer spectra

Sample	Fe^{2+}				Fe^{3+}			
	δ	Δ	Γ	I	δ	Δ	Γ	I
1 Thuringite	1.13	2.62	0.36	75	0.36	0.74	0.68	25
2 Chamosite	1.15	2.62	0.38	88	0.45	0.76	0.60	12
3 Ripidolite	1.13	2.62	0.32	84	0.45	0.71	0.55	16
4 Clinochlore	1.13	2.61	0.36	79	0.40	0.61	0.48	21
5 Amesite	1.12	2.60	0.32	60	0.32	0.49	0.48	40
Minnesotaite	1.15	2.75	0.36	92	0.26	0.40	0.37	8
Ferrobrucite	1.16	2.95	0.30	70	0.33	0.63	0.63	30

δ: Isomer shift relative to metallic iron (mm/s); Δ: Quadrupole splitting (mm/s); Γ: Full width at half-maximum (mm/s); I: Relative intensity (%)

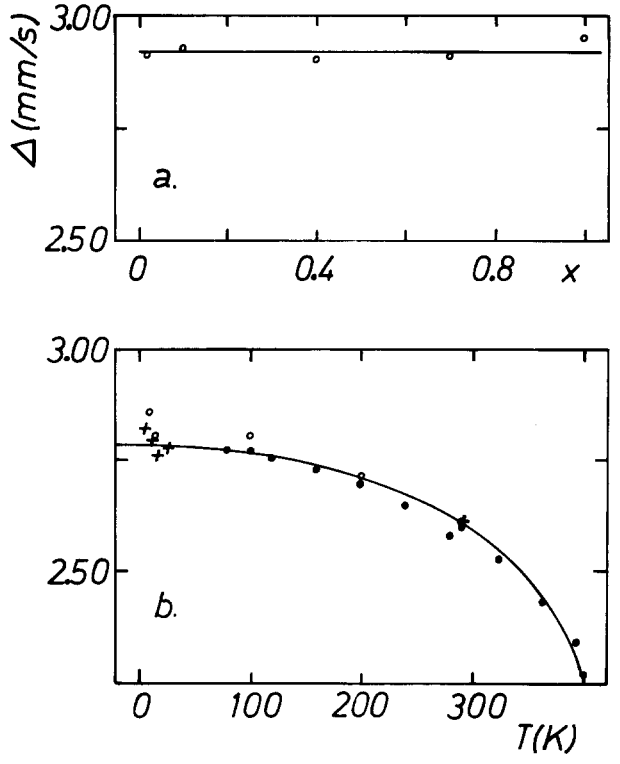

Fig. 3. (**a**) Quadrupole splitting of $Fe_xMg_{1-x}(OH)_2$ solid solutions as a function of x. (**b**) Quadrupole splitting for chlorites as a function of temperature: o thuringite, + chamosite, • clinochlore

ium-rich 2*H* serpentine mineral rather than a true chlorite. Lattice parameters are $a=5.32$ Å, $b=9.21$ Å, $c=14.06$ Å (Steinfink and Brunton 1956).

The Fe^{2+}:Fe^{3+} ratios in all the above formulae were obtained from the room-temperature Mössbauer spectra shown in Fig. 2, assuming identical recoilless fractions for the two valence states. These spectra are all remarkably similar in view of the enormous variation in iron content. Hyperfine parameters are given in Table 1. The ferrous lines have a width of 0.32–0.38 mm/s, and so the different octahedral sites are indistinguishable although both *M*1, *M*2 and *M*3 must be occupied, at least in sample 1 because of its high iron content. This point is discussed further below. Even the spectrum of the 1:1 layer mineral chamosite is undifferentiated from the others. Neither the cation nor anion neighbours appear to have a decisive effect on the ferrous quadrupole doublet in chlorites. It is particularly remarkable that octahedral sites with two (*M*1, *M*2), four (chamosite) or six (*M*3) hydroxyls give the same ferrous spectrum.

The parameters of the ferrous talc, minnesotaite $\delta=1.15$, $\Delta=2.75$, $\Gamma=0.36$ mm/s and normal talc $\delta=1.13$, $\Delta=2.64$, $\Gamma=0.30$ are a little different from those of the ferrous doublet in chlorites. We also made solid solutions $Fe_xMg_{1-x}(OH)_2$ $0.1\leq x\leq 1$ by precipitation from solution with KOH. Their room temperature ferrous isomer shift and quadrupole splitting (shown in Fig. 3a) are constant across the series. Δ was found to be 2.91 mm/s in a natural brucite containing 1 percent iron impurity and 2.95 mm/s in $Fe(OH)_2$ in agreement with previous work (Miyamoto et al. 1967, Blaauw et al. 1979) but significantly different from the ferrous splitting in chlorite. Our precipitates were partially oxidized, and some representative ferric parameters are included in Table 1.

Magnetic Properties

The magnetic measurements, and the procedure for analysing the magnetic susceptibility of minerals containing ferrous and ferric iron have been fully described in II. Susceptibility of powder samples follows a Curie-Weiss law, and data on the two most iron-rich samples are shown in Fig. 4a. Intercepts on the temperature axis are positive, as for the other ferrous sheet silicates featured in I and II, indicating that the exchange coupling is predominantly ferromagnetic. From the values of the paramagnetic Curie temperature θ_p, 17 K for thuringite and 12 K for chamosite, the average exchange constants J are derived as 1.2 K and 1.1 K respectively.

The anisotropic susceptibility, measured parallel and perpendicular to the **c**′ direction normal to the layers of the clinochlore sample which contains relatively little iron, is shown in Fig. 4b. The anisotropy is similar to that reported in II for a ferrous vermiculite and the experimental parameters deduced from fitting the data in the same way as in II were the following: the ferric fraction $p_3=0.23$, the empirical Curie-Weiss parameters in the equation $\chi_\alpha=C_\alpha/(T-\theta_\alpha)=-13$ K, $\theta_\perp=7$ K, $C_\parallel=4.0\times10^{-3}$ emu/g, $C_\perp=4.4\times10^{-3}$ emu/g, and the derived parameters appropriate for Fe^{2+} alone, denoted by (2), are $(\theta_\perp^{(2)}-\theta_\parallel^{(2)})=30(4)$ K, and $(g_\perp^{(2)}/g_\parallel^{(2)})=1.08(2)$. In the uniaxial model for Fe^{2+} in effective trigonal symmetry, which we developed in I and II for the magnetic properties of the other families

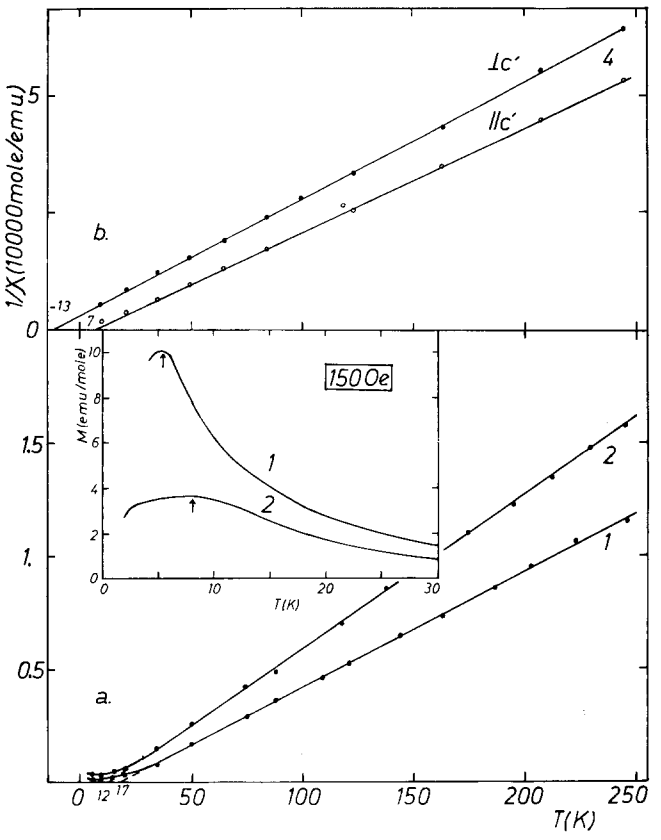

Fig. 4a, b. Inverse susceptibility (**a**) for thuringite (1) and chamosite (2). (The insert shows the magnetization of the samples measured in 150 Oe) and (**b**) for clinochlore with the field ∥ or ⊥ to *c*

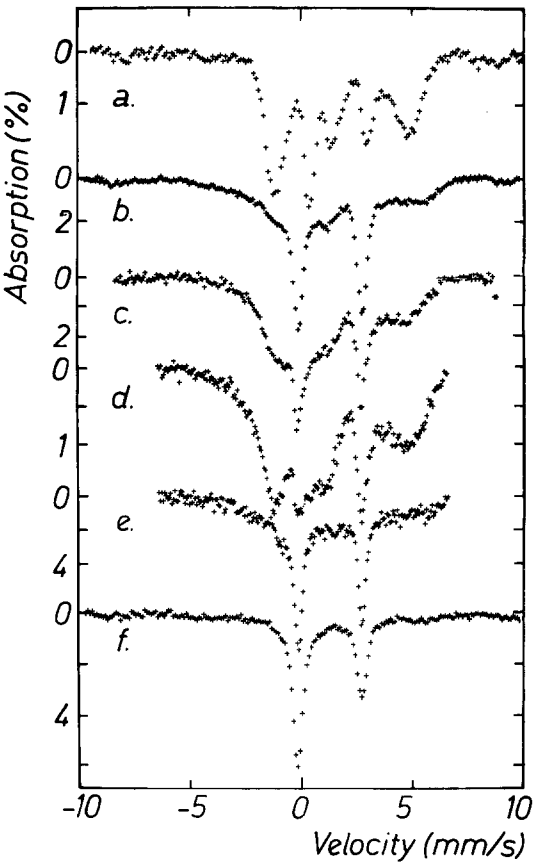

Fig. 5. Low temperature Mössbauer spectra: (a) minnesotaite at 4.2 K, (b) thuringite at 4.2 K, (c) chamosite at 4.2 K, (d) chamosite at 1.5 K, (e) ripidolite at 1.5 K, (f) clinochlore mosaic with $\gamma \parallel c'$ at 4.2 K

of sheet silicates, the trigonal splitting δ_t is 1,120 K. This value compares favourably with that deduced from the temperature dependence of the quadrupole splitting shown in Fig. 3b ($\delta_t = 1{,}150$ K), although the fit there is only fair.

The iron-rich samples exhibit a maximum in their magnetic susceptibility in low fields at a temperature T_m which would normally be associated with the onset of magnetic ordering. The peak for thuringite is sharper than that for chamosite, as may be seen in the insert in Fig. 4a. The onset of magnetic hyperfine splitting in the Mössbauer spectrum takes place near the temperature of the susceptibility maximum. some low-temperature spectra are shown in Fig. 5, where that of minnesotaite, which orders at 28 K is included for reference. The notable feature for the iron-rich chlorites is that the paramagnetic ferrous peaks persist to some extent at temperatures well below that of the susceptibility maximum, T_m. They are much more pronounced for thuringite than for chamosite, even though the former has greater iron content. These paramagnetic peaks are practically absent from the spectrum of minnesotaite, which is composed of ferrous talc layers. Ferric iron also shows hyperfine splitting at 4.2 K in the spectra of Fig. 5a and b. Ferrous hyperfine structure is broadly similar in those samples where it appears, but only the 4.2 K minnesotaite spectrum and the 1.5 K chamosite spectrum were well enough resolved to be successfully computer-fitted. Resulting hyperfine parameters were $\delta = 1.35(2)$ mm/s, $\Delta = -3.05(6)$ mm/s, $\eta = 0.10(5)$ and $H_{hf} = 130(3)$ kOe for minnesotaite and $\delta = 1.36(2)$ mm/s, $\Delta = -2.78(8)$ mm/s, $\eta = 0.00(5)$ and $H_{hf} = 142(3)$ kOe for chamosite.

High-field magnetization curves for all five samples at 4.2 K are shown on Fig. 6. Those in Fig. 6a for the powder specimens show that the magnetization of thuringite, chamosite, ripidolite and amesite approaches saturation in a field of 150 kOe: Saturation magnetization expected of these four samples is 132, 111, 81, and 2,5 emu/g, in order of decreasing iron content. Extrapolating the data above 130 kOe to $1/H = 0$ yields values of 110, 90, 65 and 1 emu/g, respectively. This discrepancy suggests that a number of strong antiferromagnetic bonds are present. The curves measured in the two directions for clinochlore crystals for which the saturation magnetization is 29 emu/g are given in Fig. 6b, together with the theoretical curves calculated from a trigonal crystal-field model for the Fe^{2+} ion described in II. Agreement here is quite good.

Powder neutron diffraction data (Fig. 7) were obtained on thuringite at the Institut Laue Langevin, Grenoble. Experimental details are given in I. Two diagrams taken at temperatures well above and well below T_m, at 27 K and 1.6 K, turned out to be almost identical as shown by the difference diagram in Fig. 7b. No magnetic Bragg scattering appeared, whether at the positions of the nuclear peaks or as superlattice reflexions. The only difference between the two diagrams was an increase in the small-angle scattering at 1.6 K, as shown in Fig. 7b. Corresponding measurements were made on a biotite sample similar to biotite 2

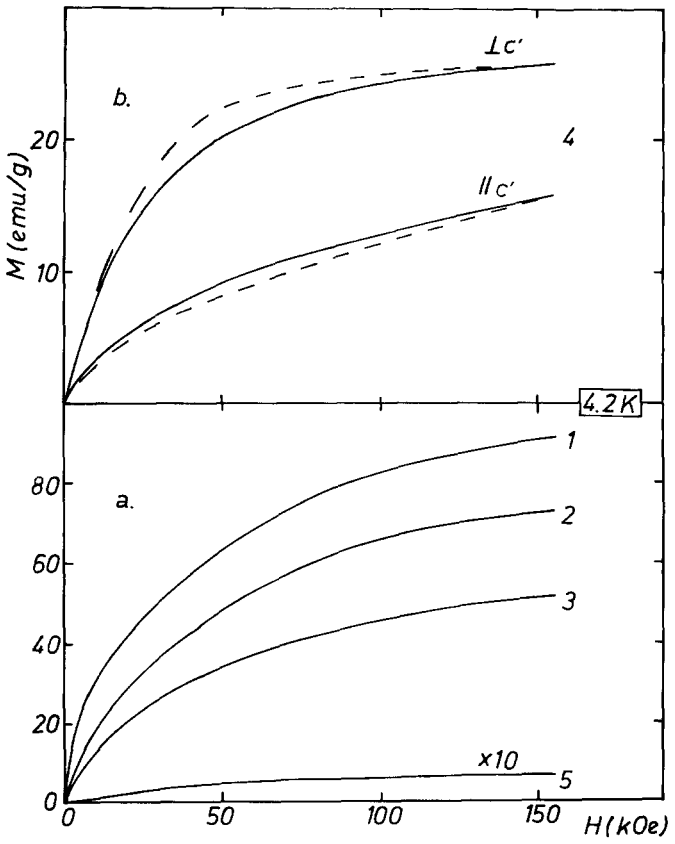

Fig. 6a, b. High-field magnetization curves at 4.2 K: (**a**) for powders of thuringite (1) chamosite (2) ripidolite (3) and amesite (5), (**b**) for clinochlore with the field ∥ or ⊥ to the **c**′ direction normal to the sheets. The dashed line is the calculation described in the text

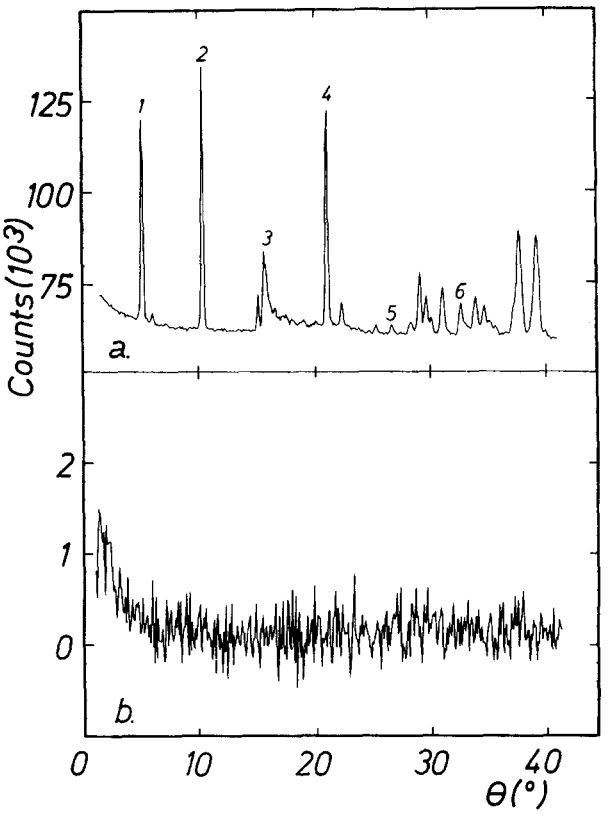

Fig. 7. (**a**) Powder neutron diffraction pattern of thuringite at 27 K. The first six 00*l* reflections are marked by figures. (**b**) Difference diagram showing the neutron scattering at 1.6 K less that at 27 K

of paper II, which has $T_m = 7$ K and shows magnetic hyperfine splitting below that temperature, with identical results[1]. By contrast, both greenalite (Coey et al. 1981) and minnesotaite (Ballet et al. 1985) exhibit a set of magnetic superlattice reflexions of the type $hk(2l+1)/2$ due to the antiferromagnetic ordering of successive ferromagnetic octahedral sheets. In both these minerals the $00\frac{1}{2}$ magnetic peak is more intense than the most intense nuclear peak, so it is all the more remarkable that nothing of the kind appears for thuringite or biotite. Unfortunately, the ferromagnetic correlation length cannot be inferred precisely from the small angle scattering which varies as $1/\theta$, corresponding to the geometrical Lorentz factor.

Table 2. Observed intensities for the (00*l*) nuclear reflections in thuringite compared with the results of calculations with various values of the talc-brucite iron distribution parameter *D*

I_{obs}		I_{calc}			
		$D=2.33$	$D=0.2$	$D=0$	$D=-2.33$
001	62 (5)	163	61	54	4
002	78 (5)	78	78	78	78
003	35 (11)	13	29	30	53
004	70 (5)	77	77	77	77
005	3.2 (3)	9	4	3	0
006	16 (4)	14	14	14	14

Discussion

The distribution of iron between the talc and brucite layers in sample 1 can be deduced by analysing the 00*l* Bragg peaks in the neutron diffraction diagram, Fig. 7a. We calculated the structure factors of the 00*l* reflections, taking the *z* parameters for the atomic positions including that of hydrogen from the neutron structure determination of a penninite by Joswig et al. (1980). The intensities of the 00*l* reflections with *l* even are independent of cation distribution, and, as shown in Table 2, experimental values agree well with the calculated ones. However, the 00*l* reflections with *l* odd are particularly sensitive to the iron distribution because the iron scattering length is roughly double that of Mg or Al. Defining the difference in the numbers of iron in the talc and brucite layers as *D*, calculated intensities are given in Table 2 for two extremes, $D = \pm 2.33$, corresponding to total occupancy of the talc or brucite sheets by Fe, as well as $D=0$, a random distribution of cations over the two sheets and $D=0.2$, the value that best fits the observed 00*l* intensities. We therefore estimate $D=$

1 Analysis of the biotite 2 magnetization curve in II in terms of a spin flop transition must be discounted in view of this new information

Table 3. Magnetic properties of trioctahedral ferrous sheet silicates

Mineral	Layer	Sheet spacing (Å)	Z	θ_p (K)	T_m (K)	θ/T_m	p_3 (%)	p_{33} (%)	Magnetic order	Reference
Ferrobrucite*	1	4.6	6.0	30	34	0.9	0	0	af	Miyamoto (1976)
Greenalite	1:1	7.2	5.2	24	17	1.4	12	3	af	Ballet (1979)
Chamosite	1:1	7.1	3.0	12	~8	~1.5	12	1		This work
Minnesotaite	2:1	9.6	4.5	38	19	2.0	8	1	af	Ballet et al. (1985)
Biotite	2:1	10.0	5.3	43	7	6.1	13	4	rf	Ballet and Coey (1982)
Thuringite	2:1:1	7.1	3.9	17	5	3.4	25	8	rf	This work

* synthetic $Fe(OH)_2$; af = antiferromagnetic; rf = random ferromagnetic; Z number of iron nearest-neighbours of a site in the octahedral sheet; p_3 ferric fraction of total iron; p_{33} probability that two adjacent octahedral sites are occupied by Fe^{3+}

0.2(3), indicating that 1.9(3) iron ions/formula are in the talc sheet and 1.7(3) are in the brucite sheet. Since the formula only contains 0.9 Fe^{3+} ions, it follows that a significant amount of Fe^{2+} must lie in the brucite sheet.

The magnetic properties of the chlorites that are low in iron, and therefore exhibit no collective magnetic order, are similar to those of the low-iron trioctahedral 2:1 minerals described in II. The key to understanding their magnetocrystalline anisotropy is the orbital ground state of the Fe^{2+} ion in its octahedral sites. There is plenty of convergent evidence that the ferrous iron in sheet silicates may be regarded as having an orbital singlet ground state due to an effectively trigonal point symmetry that would result from compression of the oxygen octahedra in the **c′** direction, normal to the layers. This model provides for hard **c′** axis anisotropy and can explain, in a semiquantitative way, the temperature dependence of the susceptibility and the field dependence of the magnetization measured parallel and perpendicular to **c′**, as well as the sign and magnitude of the electric field gradient parameters V_{zz} and η (−3 mm/s and 0, respectively) and the temperature dependence of the quadrupole splitting. Nevertheless, it is only a working hypothesis and surely cannot be correct in detail as there is no three-fold axis in the point symmetry of $M1$, $M2$ or $M3$ sites. There will be terms in the crystal field which separate all three energy levels issuing from the T_{2g} triplet, and produce in-plane anisotropy for example, or cause the hard axis to deviate from **c′**. The crystal field will actually be different at every atomic site in a natural silicate because of different local cation environments.

Turning now to trioctahedral sheet silicates richer in ferrous iron, the average paramagnetic Curie temperature θ_p is positive (see Fig. 4a). Values for the average exchange constant J of 1.2 K and 1.1 K respectively, were deduced above for thuringite and chamosite. These values are quite similar to that found earlier for biotite (2.0 K), and confirm the ferromagnetic character of the dominant exchange coupling in chlorites, as in other trioctahedral ferrous minerals, which results from the near −90° Fe^{2+}—O—Fe^{2+} superexchange bond angles.

Besides the cation distribution, the main lesson to be learnt from the neutron results on chlorite and biotite is that a peak in the low-temperature susceptibility and the appearance of magnetic hyperfine splitting in the Mössbauer spectrum do not *necessarily* imply that there is any long-range magnetic order. Nevertheless, some sheet silicates undoubtedly do exhibit long-range planar antiferromagnetic order. So what is the reason? Relevant data on five sheet silicates are summarized in Table 3, together with results on synthetic $Fe(OH)_2$, whose structure may be regarded simply as a stack of octahedral sheets with no tetrahedral silicate sheets between them. From the Table it seems that $\theta_p/\mathbf{T}_m$ is a critical quantity. Long-range antiferromagnetic ordering occurs when $\theta_p/T_m < 2$, but if $\theta_p/T_m > 3$ there is only short range ferromagnetic ordering within the sheets.

Two factors are potentially relevant in determining whether long-range magnetic order occurs or not. One is the strength of the interplane antiferromagnetic coupling. If this were truly insignificant, a perfect trioctahedral ferrous sheet with hard axis (easy plane) anisotropy would resemble the ferromagnetic $2dXY$ model at low temperature. It is predicted theoretically that this model never exhibits long-range order, but that the spins freeze into a vortex state below a finite temperature T_{TK} below which the susceptibility diverges (Kosterlitz and Thouless 1973). Increased intersheet spacing, while likely to destabilize the antiferromagnetic state by reducing the intersheet interaction, does not by itself account for the results in Table 3. Materials with octahedral intersheet spacings of 4.6, 7.2 and 9.6 Å order antiferromagnetically yet others with spacings of 7.1 and 10.0 do not. (The thuringite spacing is 7.1 Å because iron is present in both talc and brucite sheets).

The other factor that tends to destroy the antiferromagnetic state, because it weakens the ferromagnetic coupling in the plane, is ferric iron. All the natural minerals in Table 3 contain some ferric iron, up to 25% of the total iron. The ferric fraction p_3 is listed in the Table. If Fe^{2+}—O—Fe^{2+} superexchange in the octahedral sheet is certainly positive, and the Fe^{2+}—Fe^{3+} interaction probably so (see the example of glauconite in paper II), the Fe^{3+}—O—Fe^{3+} interaction in the octahedral sheet is certainly negative (Coey et al. 1984). It follows that isolated Fe^{3+} ions will not break up the ferromagnetism in the sheets, but Fe^{3+}—Fe^{3+} nearest-neighbour pairs may have a disasterous effect, particularly if there is already some tendency to form vortices. In Table 3, Z is the average number of iron neighbours of an octahedral site (maximum 6 for the iron end-members where the probability of octahedral iron site occupancy is 1). When the octahedral cations in the formulae derived by chemical analysis fall short of six, their number was normalized to six to calculate Z. The parameter p_{33}, defined as $1/12\ (p_3\ Z)^2$, represents the probability that an octahedral site will be occupied by a ferric ion belonging to an Fe^{3+}—Fe^{3+} pair, assuming a random cation distribution. In the planar antiferromagnetic minerals this probability does not exceed 3 percent, but the two for which we

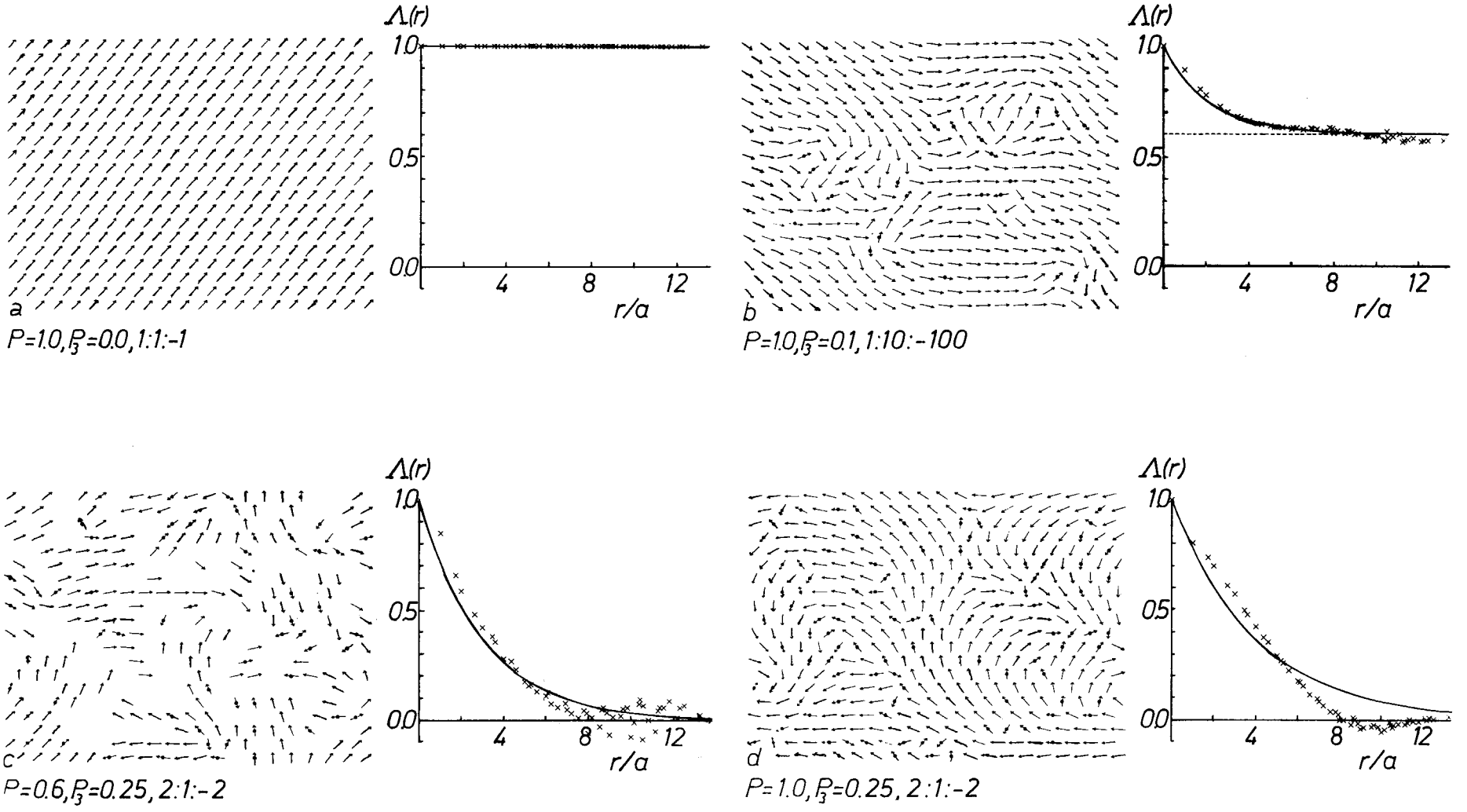

Fig. 8a–d. Monte Carlo ground states of a 400 sites triangular lattice with $2d$ vector moments. Iron ions are represented by arrows, with circles denoting ferric ions. Below each diagram are listed p the probability of site occupancy by iron, p_3 the probability that the iron is Fe^{3+} and the ratio of the coupling strengths $J_{2+2+}:J_{2+3+}:J_{3+3+}$. The cross-correlation function $\Lambda(r)$ is shown in each case

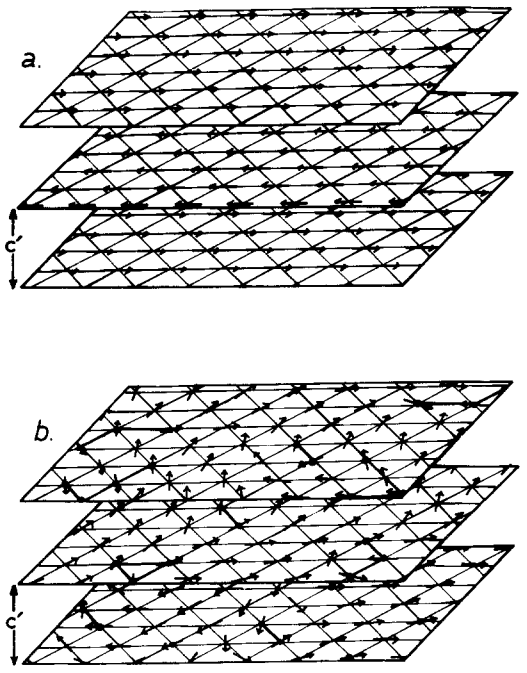

Fig. 9a, b. Two types of magnetic order that occur in predominantly ferrous trioctahedral sheet silicates (**a**) planar antiferromagnetism and (**b**) a random spin structure with short-range ferromagnetic correlations within the planes, but no correlations between them. In these illustrations all sites are supposed to be occupied by iron, but ferric ions in **b** are denoted by open circles. Ferromagnetism is destroyed by the Fe^{3+}—Fe^{3+} pairs which are indicated by the solid lines

find only ferromagnetic short-range order in the plane have $p_{33} > 4$ percent.

In order to study the influence of nonmagnetic ions and Fe^{3+}—Fe^{3+} pairs on the magnetic ground state of a layer of octahedral sites in trioctahedral sheet silicates, a Monte Carlo program was devised to simulate the behaviour of two-dimensional classical magnetic moments on a triangular lattice. In this program, the lattice is randomly populated with given concentrations of Fe^{2+} and Fe^{3+} ions, and the relative coupling strengths of the Fe^{2+}—Fe^{2+}, Fe^{2+}—Fe^{3+} interactions are specified. A random orientation between 0 and 2π is assigned to each ion, representing the direction of its magnetic moment. Then any occupied site is selected, and a random change is made in the orientation of the ion. If a decrease in the total energy of the lattice results, the new orientation is retained; otherwise, it reverts to its original value. This process is repeated until the size of the average change in orientation is very small and the total energy converges; for a 400-site array, approximately 4000 such steps per site were required. The orientations of the ions then represent the ground state of the lattice for the given distribution of ions and vacancies, and a particular ratio of coupling strengths.

For such a lattice, the correlation function is defined as

$$\Gamma(r) = \langle (\mathbf{m}_i - \langle \mathbf{m} \rangle) \cdot (\mathbf{m}_j - \langle \mathbf{m} \rangle) \rangle$$

where $\langle \mathbf{m} \rangle$ = average magnetisation (over all ions); $\mathbf{m}_k$ = the magnetic moment of the kth ion; r = distance between the ith and jth ions; $\langle \ldots \rangle$ = average over all ions.

This reduces to

$$\Gamma(r) = \Lambda(r) - \langle m \rangle^2$$

where $\Lambda(r) = \langle \mathbf{m}_i \, \mathbf{m}_j \rangle$, the cross-correlation function.

For a sufficiently large lattice, $\Gamma(r)$ will depend only on the concentrations of ions and vacancies, and relative coupling strengths, and not on their particular random distribution. It is expected to be of the form

$$\Gamma(r) = \Gamma(0)\, e^{-r/\xi}$$

where ξ is the magnetic correlation length, and so

$$\Lambda(r) = \Gamma(0)\, e^{-r/\xi} + \langle m \rangle^2.$$

The results of four individual runs of the program are shown in Fig. 8. Figure 8(a) shows the lattice populated completely by Fe^{2+}. It is totally ferromagnetic, as indicated by the cross-correlation function. Figure 8(b) illustrates the effect of a small cconcentration of Fe^{3+} ions which have strong antiferromagnetic Fe^{3+}—Fe^{3+} coupling. Fe^{3+} ion pairs lead to vortices in the magnetic structure. The correlation length is now finite, and the average magnetisation less than unity. Figure 8(c) shows the result of a typical simulation where the parameters p, p_3 and the ratio of coupling strengths are chosen to correspond to those in the real material, thuringite. The correlation function here indicates that ferromagnetic correlation is present over distances of order 10 Å (the interatomic spacing in thuringite is 3.2 Å) but there is no long-range ferromagnetic order since the cross-correlation function tends to zero. Nonmagnetic ions on octahedral sites ($p < 1$) also seem to help destabilize the ferromagnetic ground state provided Fe^{3+} is present. For Fig. 8(d) the same values of p_3 and the coupling strengths are chosen as for 8(c), but $p = 1$. However, in the absence of vacancies, different runs give a cross-correlation function which may tend towards a positive, negative or zero limit. A much larger lattice would be needed to achieve consistent results.

In summary, two possible forms of magnetic order are possible in largely ferrous trioctahedral sheet silicates. They are illustrated schematically in Fig. 9. The main factor which tips the balance between one and the other appears to be the quantity of ferric iron present in the sheets.

Conclusions

1. The trigonal model is a good first approximation for understanding the magnetic properties of all sheet silicates containing ferrous iron. It could however be improved upon if the complete orientational dependence of the susceptibility of pure (preferably synthetic) crystals doped with a little Fe^{2+} was known.

2. Two sorts of magnetic order can occur in trioctahedral ferrous sheet silicates (i) planar antiferromagnetism, with the Fe^{2+} moments lying in the ferromagnetic sheets and (ii) random spin freezing, again with the moments in the plane of the sheets, but with only short-range ferromagnetic correlations over distances of order ξ. In both cases, there is hysteresis well below T_m, the susceptibility peaks at a high value at T_m, and magnetic hyperfine splitting appears at lower temperatures. It cannot be assumed that these features necessarily indicate long-range antiferromagnetic order.

3. The critical factor determining the magnetic ground state is not so much the intersheet spacing (although the origin of the negative intersheet coupling is still unclear) as the presence of Fe^{3+} pairs in the sheets together with vacancies. Computer simulations show clearly the formation of vortices around these pairs.

4. The interest of sheet silicates from a magnetic point of view has now been established. Further progress in understanding their magnetic structures requires laboratory work on synthetic crystals of controlled composition with a view, for example, to determining the magnetic phase diagram as a function of iron concentration p, ferric iron content p_3, and intersheet spacing, in conjunction with further computer experimentation.

Acknowledgements. We are grateful to P Mangin for helping us obtain the neutron diffraction patterns at the ILL. The high field magnetization measurements were made at the Service National des Champs Intenses, Grenoble and some of the other measurements were made when OB and JMDC were at the Groupe des Transitions de Phases, CNRS Grenoble. Part of this work was supported by the National Board of Science and Technology under grant No SRP 117/84

References

Bailey SW (1980) Structures of layer silicates. In: Brindley GW, Brown G (eds) Crystal structures of clay minerals and their X-ray identification. Mineralogical Society, London, pp 1–124

Ballet O (1979) Fe^{2+} dans les silicates lamellaires: Étude magnétique et Mössbauer. Thèse de Troisième Cycle, Grenoble

Ballet O, Coey JMD (1982) Magnetic properties of sheet silicates; 2:1 layer minerals. Phys Chem Minerals 8:218–229 (Paper II)

Ballet O, Coey JMD, Mangin P, Townsend MG (1985) Ferrous talc – a planar antiferromagnet. Solid State Commun 55:787–790

Blaauw C, Stroik G, Leiper W (1980) Mössbauer analysis of talc and chlorite. J Physique 41:Cl 411–412

Blaauw C, Stroink G, Leiper W, Zentilli M (1979) Crystal-field properties of iron in brucite. Phys Status Solidi b92:639–643

Borggard OK, Lindgreen HB, Mrup S (1982) Oxidation and reduction of structural iron in chlorite at 480° C. Clays Clay Miner 30:353–364

Brown G, Brindley GW (1980) X-ray diffraction procedures for clay mineral identification. In: Brindley GW, Brown G (eds). Crystal structures of clay minerals and their X-ray identification. Mineralogical Society, London, pp 305–306

Coey JMD (1984) Silicate Minerals. In: Long CJ (ed) Chemical Applications of Mössbauer Spectroscopy , vol 1. Plenum, New York, Ch 14, pp 443–509

Coey JMD, Ballet O, Moukarika A, Soubeyroux JL (1981) Magnetic properties of sheet silicates; 1:1 layer minerals. Phys Chem Minerals 7:141–148 (Paper I)

Coey JMD, Chukhrov FV, Zvyagin BB (1984) Cation distribution, Mössbauer spectra and magnetic properties of ferripyrophyllite. Clays and Clay Minerals 32:198–204

Foster MD (1962) Interpretation of the composition and a classification of the chlorites. Prof Pap US Geol Surv:414-A, 1–33

Goodman BA, Bain DC (1979) Mössbauer spectra of chlorites and their decomposition products. In: Mortland MM, Farmer VC (eds) Proc Inst Clay Conf, Oxford 1978. Elsevier, Amsterdam, pp 65–74

Hayashi H, Sano H, Shirozu H (1972) Mössbauer spectra of chlorites in natural and heated states. Kobutzugaku Zasshi 10:507–516 (in Japanese)

Joswig W, Fuess H, Rothbauer R, Takeuchi Y, Mason SA (1980) A neutron diffraction study of a one-layer triclinic chlorite (penninite). Am Mineral 65:349–352

Kodama H, Longworth G, Townsend MG (1982) Mössbauer investigation of some chlorites and their oxidation products. Can Mineral 20:585–592

Kosterlitz JM, Thouless DJ (1973) Ordering, metastability and phase transitions in two-dimensional systems. J Phys C6:1181–1203

Miyamoto H, Shinjo T, Bando Y, Takada T (1967) Mössbauer effect of ^{57}Fe in $Fe(OH)_2$. Bull Inst Chem Res Kyoto Univ 45:331–341

Miyamoto H (1976) Magnetic properties of $Fe(OH)_2$. Mater Res Bull 11:329–333

Petruk W (1964) Determination of the heavy atom content in chlorite by means of the X-ray diffractometer. Am Mineral 49:53–71

Petruk W (1965) Relationship between the specific magnetic susceptibility and the iron plus manganese content of chlorite. Can Mineral 8:372–376

Ross GJ, Kodama H (1976) Experimental transformation of a chlorite into a vermiculite. Clays Clay Miner 22:205–211

Steinfink H, Brunton G (1956) The crystal structure of amesite. Acta Crystallogr 9:487–492

Townsend MG, Longworth G, Kodama H (unpublished) Magnetic interaction at low temperature in chlorites and their oxidation products. A Mössbauer investigation

Townsend MG, Longworth G, Roudaut E (1985) Field-induced ferromagnetism in minnesotaite. Phys Chem Minerals 12:9–12

Received April 30, 1985